

r-process Enrichment of the Ultra-faint Dwarf Galaxies by Fast-merging Double-neutron Stars

Mohammadtaher Safarzadeh¹, Enrico Ramirez-Ruiz^{2,3}, Jeff. J. Andrews^{3,4,5}, Phillip Macias², Tassos Fragos⁶, and Evan Scannapieco¹

School of Earth and Space Exploration, Arizona State University, USA; mts@asu.edu
 Department of Astronomy and Astrophysics, University of California, Santa Cruz, CA 95064, USA
 Niels Bohr Institute, Blegdamsvej 17, DK-2100 København Ø, Denmark
 Foundation for Research and Technology-Hellas, 100 Nikolaou Plastira St., 71110 Heraklion, Crete, Greece
 Physics Department & Institute of Theoretical & Computational Physics, University of Crete, 71003 Heraklion, Crete, Greece
 Geneva Observatory, University of Geneva, Chemin des Maillettes 51, 1290 Sauverny, Switzerland
 Received 2018 October 5; revised 2019 January 10; accepted 2019 January 11; published 2019 February 14

Abstract

The recent aLIGO/aVirgo discovery of gravitational waves from the neutron star merger (NSM) GW170817 and the follow-up kilonova observations have shown that NSMs produce copious amounts of *r*-process material. However, it is difficult to reconcile the large natal kicks and long average merging times of double-neutron stars (DNSs) with the levels of *r*-process enrichment seen in ultra-faint dwarf (UFD) galaxies such as Reticulum II and Tucana III. Assuming that such dwarf systems have lost a significant fraction of their stellar mass through tidal stripping, we conclude that contrary to most current models, it is the DNSs with rather large natal kicks but very short merging timescales that can enrich UFD-type galaxies. These binaries are either on highly eccentric orbits or form with very short separations due to an additional mass transfer between the first-born neutron star and a naked helium star, the progenitor of the second neutron star. These DNSs are born with a frequency that agrees with the statistics of the *r*-process UFDs, and merge well within the virial radius of their host halos, therefore contributing significantly to their *r*-process enrichment.

Key words: galaxies: dwarf – stars: evolution – stars: neutron

1. Introduction

The recent aLIGO/aVirgo discovery of a neutron star merger (NSM) GW170817 (Abbott et al. 2017a) and the subsequent kilonova observed across the entire electromagnetic spectrum (Abbott et al. 2017b; Coulter et al. 2017; Drout et al. 2017; Margutti et al. 2018) has undoubtedly shown that NSMs produce *r*-process elements in copious amounts (Kasen et al. 2017). Prior to this discovery, two ultra-faint dwarf (UFD) galaxies, Reticulum II (Ji et al. 2016), and Tucana III (Hansen et al. 2017), had been observed to be enriched in *r*-process elements, the statistics of which could be explained with a single rare event such as an NSM. These galaxies were discovered by the Dark Energy Survey (Drlica-Wagner et al. 2015; Koposov et al. 2015a), and are the only two UFDs known to show substantial *r*-process enrichment, despite observational efforts to identify others (Ji et al. 2019).

UFDs (Brown et al. 2012; Frebel & Bromm 2012; Vargas et al. 2013) are satellites of the Milky Way that are highly dark-matter-dominated (Simon & Geha 2007), with total luminosities of $L_{\star} \approx 10^3 - 10^5 \, L_{\odot}$, and they were discovered in deep wide-area sky surveys (Bechtol et al. 2015; Koposov et al. 2015a, 2015b). Based on color–magnitude diagram analysis, Brown et al. (2014) found that nearly three-fourths of the entire stellar mass content of such galaxies is formed by $z \approx 10$ and $\approx 80\%$ of the stellar mass content is already formed by $z \approx 6$.

It has been challenging to explain the observed r-process enrichment of UFDs with NSM events for two reasons: (i) UFD halo progenitors have shallow potential wells, corresponding to halo masses, $M_{\rm h}$, between 10^8 and $10^9 M_{\odot}$, depending on the assumed dark matter density profile (Simon & Geha 2007; Bovill & Ricotti 2009; Bland-Hawthorn et al. 2015). The halo mass probability density function (PDF) of

UFD progenitors has a maximum of $M_h \approx 10^9 \, M_\odot$ at redshifts around $z \approx 10$ (Safarzadeh et al. 2018). Such halos have escape velocities $v_{\rm esc} \approx 25 \, {\rm km \, s^{-1}}$, with the majority of halos of plausible UFD progenitors having $v_{\rm esc}$ less than $10 \, {\rm km \, s^{-1}}$. (ii) NSs are born with kicks that may be as large as hundreds of km s⁻¹ (Hobbs et al. 2005; Janka 2017). Although there is evidence that at least some NSs receive lower kicks at birth (e.g., Pfahl et al. 2002; van den Heuvel 2007; Verbunt et al. 2017), five of the six double-neutron stars (DNSs) with 3D velocities provided by Tauris et al. (2017) have peculiar velocities larger than 25 km s⁻¹, which suggests they would have escaped their host halos and therefore would not contribute to their r-process enrichment if they were born in UFD-type galaxies.

To take a closer look at the issue, one must consider the history of star formation of UFD-type systems, which ceases during reionization (Bovill & Ricotti 2009, 2011; Brown et al. 2014; Weisz et al. 2014). This implies that the NSM events should have taken place less than about 1 Gyr since the start of star formation. Combined with the shallow potential well of UFD host halos, if an NSM is to be considered as a plausible source of *r*-process enrichment, a binary with a merging time of less than 1 Gyr, and an escape velocity less than 25 km s⁻¹ needs to be formed frequently in the early universe, and different theoretical studies disagree on whether such binaries could have formed in UFDs (Beniamini et al. 2016; Bramante & Linden 2016).

Separately, through cosmological zoom simulations of UFDs, Safarzadeh & Scannapieco (2017) demonstrated that a single NSM event can account for the observed *r*-process enrichment in Reticulum II, with modest assumptions regarding the europium yield in the dynamical ejecta of the NSM.

However, the authors had to make the NSM event take place in less than about 10 Myr after the onset of star formation in the UFDs so that the subsequent generation of stars can inherit the r-process ejected into the interstellar medium (ISM) before the total stellar mass of the system reaches $M_{\star} \approx 10^4 \, M_{\odot}$. The simulations were stopped when the total stellar mass reached the level required to mimic the suppression of star formation by reionization. The NSM events modeled were effectively from fast-merging DNSs with very low natal kicks. Moreover, it has been pointed out that small natal kicks can have a significant impact on r-process enrichment of UFDs (Safarzadeh & Scannapieco 2017), as well as the MW galaxy (Behroozi et al. 2014; Safarzadeh & Côté 2017).

In this study, we consider different pathways through which UFDs could have been enriched in *r*-process material. We combine our understanding of the star formation and halo assembly of such systems with publicly available population synthesis models of binary compact object formation (Dominik et al. 2012).

The structure of this work is as follows. In Section 2 we describe the population synthesis model that we have analyzed in our study. In Section 3 we present our results, showing where in the parameter space the DNS candidates are born in such models that could enrich UFD-like systems with *r*-process material. In Section 4 we discuss in detail how fast-merging DNSs are formed. In Section 5 we compare the birth rate of the candidate DNSs to observations of the *r*-process-enriched UFDs, and in Section 6 we summarize our results and discuss the future work needed to improve our understanding of *r*-process enrichment at high redshifts.

2. Method

To model the formation of DNSs, we use published results from the StarTrack (Belczynski et al. 2002, 2006, 2008) population synthesis code. These simulations are described in detail in Dominik et al. (2012) and include three major improvements over previous StarTrack versions with regards to stellar winds (Belczynski et al. 2010), common envelope (CE) formulation, and compact object formation (Fryer et al. 2012). We have analyzed the intermediate data from these simulations that are publicly available. We briefly summarize the method in this section.

Each of the models we analyze has 2×10^6 binaries, initialized by four different parameters: (i) the primary star's mass M_1 ; (ii) the mass ratio $q = M_2/M_1$, with M_2 being the mass of the secondary star; (iii) the semimajor axis a of the binary; and (iv) the eccentricity e. The masses of the primary are drawn from the Kroupa initial mass function (IMF) from 5 to 150 M_{\odot} . The mass ratio is assumed to have a flat distribution between q = 0–1 with the minimum mass of the secondary considered to be $3 M_{\odot}$. The distribution of initial binary separation is assumed to be flat in $\log(a)$, and the eccentricity is drawn from thermal equilibrium distribution $\Xi(e) = 2e$, with e ranging from 0 to 1.

2.1. Model Variations

A number of parameters are varied among the models, which are meant to parameterize the uncertainties in our understanding of binary neutron star formation. The first parameter that is varied deals with the behavior of binaries when a star enters into a CE with a Hertzsprung gap (HG) donor star; during a CE, a star enters the envelope of its companion, exchanging orbital energy to unbind the donor's envelope. For giant stars, with a clear core-envelope boundary, the end result of this process (so long as there is enough orbital energy available to keep the system from merging) is a closely bound binary comprised of the accretor star and the giant star's core. However, HG stars lack well-defined cores, and studies are inconclusive as to whether binaries entering into a CE during this phase can survive without merging (Deloye & Taam 2010). We note that allowing HG stars to survive a CE significantly increases the merger rates of double black hole binaries to a level that exceeds current LIGO constraints (Belczynski et al. 2007), although it matches NSM rate estimates (Chruslinska et al. 2018).

Two different submodels, A and B, have been analyzed, and treat CE events with HG donor stars differently. Submodel A treats HG stars such that a core could be distinguished from an envelope in their evolutionary phase, hence a successful CE ejection is possible. Submodel B assumes any system entering into a CE with a HG donor will merge. As a second parameter, the kick velocity received by an NS at birth is varied. Our standard model adopts natal kicks randomly drawn from a Maxwellian distribution with $\sigma = 265 \,\mathrm{km \, s^{-1}}$, based on the observed velocities of single Galactic pulsars (Hobbs et al. 2005), and we explore the models that adopt $\sigma = 135 \,\mathrm{km \, s}^{-1}$. We note that to match merger rate estimates from LIGO, recent binary population synthesis results suggest that DNSs are likely to be born with kick velocities that are lower than the low kick models explored in this work (Giacobbo & Mapelli 2018). Finally, we test models with two different metallicities: $Z = Z_{\odot}$ and $Z = 0.1 Z_{\odot}$.

Our naming convention divides into submodels A and B, which correspond to whether HG stars survive a CE or are assumed to merge, respectively. We further subdivide our models based on metallicity (either solar or 0.1 solar). We refer to each model as (A, B)Z(02, 002)(H, L), where the first letter denotes submodels A or B, 02 and 002 correspond to solar and tenths of solar metallicity models, and the last letters (H, L) determine whether the natal kicks to the compact objects are drawn from a Maxwellian distribution with $\sigma = (265, 135) \, \mathrm{km \, s^{-1}}$, respectively. In summary, we test two different models with four possible variations each, producing eight separate cases.

2.2. Definition of Candidate DNSs

Unlike previous studies that solely focused on the natal kicks of the DNSs to determine whether they can enrich UFDs with r-process elements (Beniamini et al. 2016; Bramante & Linden 2016), here we take a different approach: a DNS with a large systemic velocity that nevertheless merges well within the virial radius of the host halo will contribute to the r-process enrichment. Therefore, all the DNSs that satisfy $t_{\rm merge} \times v_{\rm CM} < \epsilon \times r_{\rm vir}$ are considered candidates for the enrichment of UFDs. We set $\epsilon = 0.1$, noting that the half-light radius of a galaxy is correlated with its halo virial radius as $R_e = 0.015 \, r_{\rm vir}$ (Kravtsov 2013), therefore our choice for ϵ is large enough to encompass the extended ISM of the galaxy. However, we show below that our results are rather insensitive to moderate variations in ϵ . Here, $t_{\rm merge}$ is the merging time since the formation of the DNS, $v_{\rm CM}$ is the center-of-mass velocity of the

⁷ The public data from the Synthetic Universe Project are available at: www.syntheticuniverse.org.

Table 1
Formation Rate of the DNSs in Different Models

Model	# of Candidate DNSs	# of All DNSs	Fraction
AZ002H	1041(920)	5934	18%
AZ002L	1205(1139)	9918	12%
AZ02H	678(561)	9713	7%
AZ02L	1255(1158)	15575	8%
BZ002H	52(35)	4241	1%
BZ002L	17(12)	7620	0.2%
BZ02H	112(65)	6061	2%
BZ02L	28(18)	10280	0.3%

Note. The number of DNSs formed out of 2×10^6 binaries simulated in each model. The models are described in Section 2.1. The second column shows the number of candidate DNSs, which are defined as those merging well within the virial radius of a halo with mass $10^9 \, M_\odot \, (r_{\rm vir} \approx 4.6 \, {\rm kpc})$ at z=6. The numbers in parentheses show the number of candidates that merge within the virial radius of a halo with mass $10^8 \, M_\odot \, (r_{\rm vir} \approx 1.3 \, {\rm kpc})$ at z=10. The third column indicates the total number of surviving DNSs, and the forth column shows the percentage of all the DNSs that are considered to be candidates.

binary after the formation of the DNS, and $r_{\rm vir}$ is the virial radius of the UFD host halo, which is a function of both the halo's mass and its redshift.

For our analysis, we consider a UFD host halo of $10^9 M_{\odot}$ at z=6, which has a virial radius of ≈ 4.6 kpc and escape velocity of $v_{\rm esc}\approx 44\,{\rm km\,s}^{-1}$. This halo mass corresponds to the maximum mass that a UFD progenitor can have at such redshifts based on various abundance matching techniques (Safarzadeh et al. 2018). We note that although the definition of candidate DNSs above ignores the gravitational potential of UFDs, DNSs with short merger times typically have systemic velocities in excess of $10^2\,{\rm km\,s}^{-1}$, much larger than the escape velocities of UFDs. If anything, our estimates should be considered conservative, in the sense that a contribution from the host galaxy potential would result in a deceleration of newly formed DNS.

While we present our results based on a virial radius cut of UFD host halos at high redshifts, one might wonder how sensitive our rates are to the assumptions regarding the halo mass of these systems. Moreover, if the DNSs merge far from the star-forming region of the galaxies, whether the released r-process material is recycled into the newly formed stars at high concentration to make r-process metal-poor stars remains to be explored with hydrosimulations. Safarzadeh & Scannapieco (2017) showed that the location of the NSM with respect to the star-forming region could severely affect the level of r-process enhancement that would be observed in the stars. We return to this point in the following section, where we show that the distances traveled by our DNS candidates before they merge are typically less than 100 parsecs, therefore our conclusions are robust with respect to different assumptions with regards to the virial radius of such halos at high redshifts.

3. Results

We summarize our application of DNS mergers produced by the population synthesis models of Dominik et al. (2012) to UFDs in Table 1. The first column presents different models studied in this work. The second column indicates the number of candidate binary NSs, which are defined as those that are born and merge well within the virial radius of a halo with mass $10^9\,M_\odot$ ($r_{\rm vir}\approx4.6\,{\rm kpc}$) at z=6. The numbers in parentheses

show the number of candidates that merge within the virial radius of a halo with mass $10^8 \, M_\odot$ ($r_{\rm vir} \approx 1.3 \, \rm kpc$) at z=10. The third column indicates the total number of surviving DNSs in each model.

For example, considering models with high kick velocities and metallicity $Z=0.1\,Z_\odot$, out of all the 2×10^6 binaries, 5934 DNSs survive in submodel A and 4241 survive in submodel B. The corresponding numbers of DNSs that are identified as candidate DNSs are 1116 ($\approx18.5\%$) in submodel A, and only 92 candidates ($\approx1.8\%$) in submodel B. We note that if we assume Poisson noise for the numbers here, the noise is proportional to Sqrt(N), as even for the cases where only 0.1% of all the DNSs become the candidate DNSs, the signal-to-noise ratio (S/N) is significant because the sample size is about a thousand. Therefore, although a million is not a large sample for a pop-synthesis analysis, we believe the S/N is already large enough to be secure from large statistical fluctuations.

Given the specific IMF adopted in the studies of Dominik et al. (2012), modeling 2×10^6 binaries corresponds to a total stellar mass of $\approx 3 \times 10^8 \, M_\odot$. This conversion implies that one DNS is formed in (AZ002H, BZ002H) per (5 × 10⁴, 7 × 10⁴) solar mass of stars. Subsequently, the candidate DNSs have a birth rate of one per $2.8 \times 10^5 \, M_\odot$ and $5.7 \times 10^6 \, M_\odot$, respectively.

Figure 1 shows the distribution of the candidate DNSs in purple dots (and all the DNSs in a given model in green dots) in the $t_{\rm merge}$ – $v_{\rm CM}$ plane (top row of panels), and in the semimajor axis versus eccentricity plane (bottom row of panels). The left column corresponds to model AZ002H, the middle column corresponds to BZ002H, and the right column corresponds to AZ002L.

The various clusters in these panels are formed from different DNS formation channels, and the various choices of model parameter affect both the characteristics of DNSs formed through these channels and their relative ratios (Andrews et al. 2015). The two clumps of predominantly green points (seen clearly in the top panels) are differentiated by whether the DNSs went through (stable) Case BB mass transfer during formation. Case BB mass transfer refers to when an NS accretes He from the He HG star (Delgado & Thomas 1981). Systems with wide enough separations, or those that are after the first CE phase, having a helium star with a mass larger than $3-4 M_{\odot}$, do not go through case BB mass transfer, and therefore form DNSs with separations too large to merge within a Hubble time. Alternatively, systems that go through stable Case BB mass transfer tend to form shorter period systems, a fraction of which merge quickly enough to be LIGO sources. A third formation channel exists (the dense clump of purple points in the top panels) for submodel A only, which allows for certain systems to form through unstable Case BB mass transfer. We further describe this channel-including why it only exists for submodel A—below in Section 4.2.

Figure 1 shows that there are two channels to make the candidate DNSs: (i) binaries with rather small separations in highly eccentric orbits, and (ii) binaries with small separation without bias in eccentricity. The first channel contributes to the binary formation in both submodels, while the second channel produces the majority of binaries in submodel A, but does not contribute to the formation of DNSs in submodel B. We discuss these channels in more detail in Section 4.

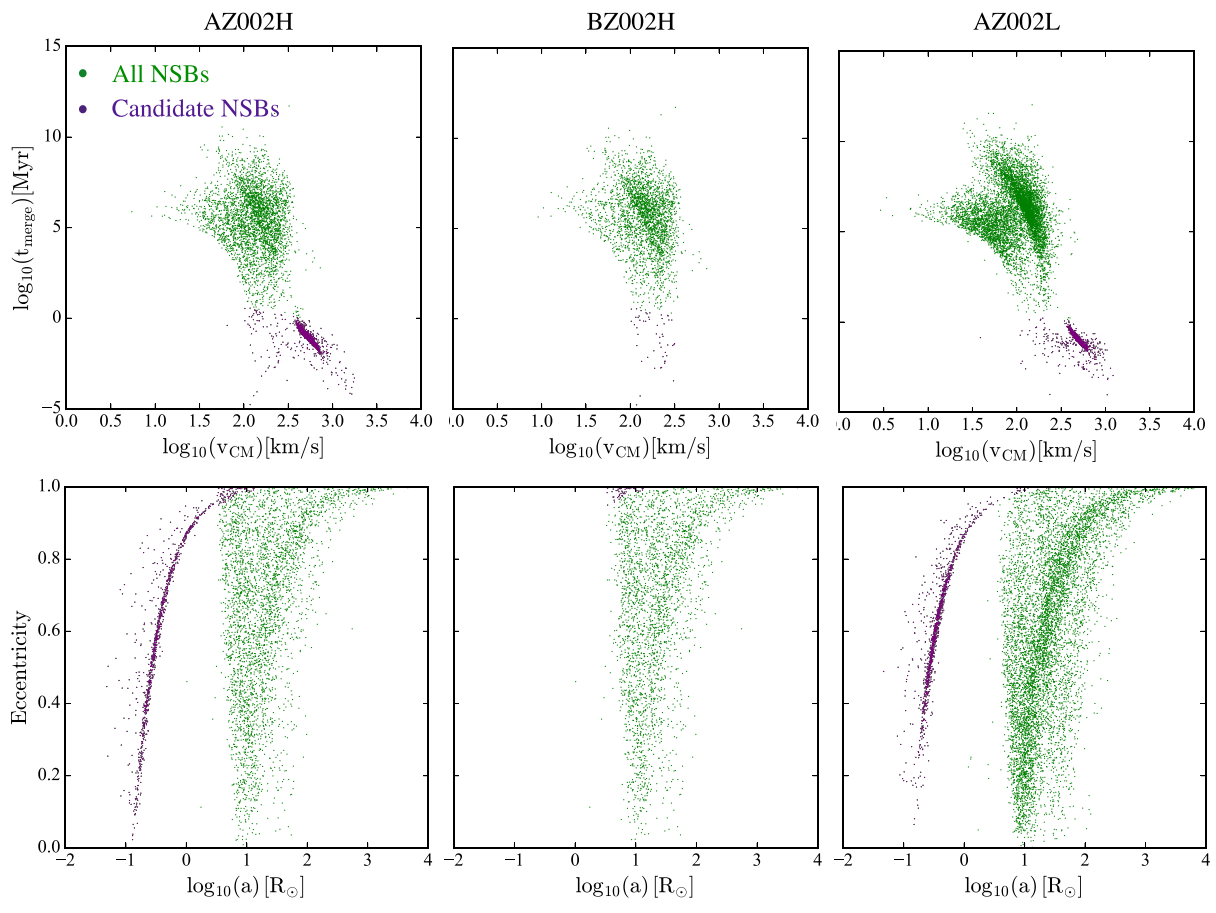


Figure 1. Distribution of DNS properties just after the formation of the second NS in the t_{merge} – v_{CM} plane (top row), and in the semimajor axis versus eccentricity plane (bottom row). The green points are all the DNSs in submodel A and the purple points are the candidate DNSs that are born in the $10^9 \, M_{\odot}$ halo at z = 6 and merge within its virial radius. The left column corresponds to submodel A, the middle column corresponds to submodel B, and the right column corresponds to a variation of the model with low natal kicks imparted to the neutron stars upon birth. Note that we are only showing the DNSs that merge in less than 10^{13} Myr, and the models are at $0.1 \, Z_{\odot}$.

Figure 2 shows the cumulative distribution function of the distance traveled by the candidate DNSs before they merge. As can be seen, about 90% of our candidates merge within the central hundred parsecs of the galaxy; even though we define our candidate DNSs as those that merge within the virial radius, most candidate DNSs merge much deeper in the potential well of the galaxy. Depending on how close the NSM event takes place to the star-forming region of a UFD, different classes of r-process-enhanced metal-poor (MP) stars (Beers & Christlieb 2005), either MP-rI (with 0.3 < [Eu/Fe] < 1) or MP-rII ([Eu/Fe] > 1), could form.

4. The Evolutionary Channels of the Fast-merging DNS Systems

It takes approximately 10–20 Myr to evolve a high-mass binary from birth to the formation of a DNS system. The subsequent time to merger due to gravitational-wave radiation varies by many orders of magnitude, but can be of the order of Myr or less. As indicated in the previous section, there are two general evolutionary scenarios for forming DNSs with short merging times:

(i) During the second SN, a system can randomly receive a kick with the right magnitude and direction to place it on a highly eccentric orbit. This occurs in a small but non-negligible fraction of DNSs, and quickly leads to a merger

 $(\lim_{e \to 1} t_{\text{merge}} = 0)$. We call this the highly eccentric orbit channel and discuss it further in Section 4.1.

(ii) During the late stages of evolution, a system can experience unstable mass transfer from a He-star donor to an NS accretor that does not lead to a merger within the CE. This evolutionary channel results in the formation of a binary system of an NS with a naked CO-core, and orbital separation $\approx 0.1\,R_\odot$. Due to their tight orbital separations, these systems likely survive the second SN, regardless of the kick velocity and direction, to form a DNS that quickly merges afterward. We call this the unstable case BB mass transfer channel and discuss it further in Section 4.2.

4.1. The Highly Eccentric Orbit Channel

After the formation of the first NS in a DNS, a typical highmass binary will evolve through one or more mass transfer phases (systems that avoid mass transfer are too widely separated to merge within a Hubble time). The first of these phases is typically a CE (MacLeod & Ramirez-Ruiz 2015), forming a tight binary comprised of an NS with a He-star companion that has lost its H-envelope. After further evolution, these "naked" He-stars begin to form a stratified structure of a carbon–oxygen (CO) core, surrounded by a He-envelope, in the process evolving through a helium HG phase. Such "naked" He HG stars typically have radii $\approx R_{\odot}$. Depending on the orbital separation, the system may enter a second phase of mass

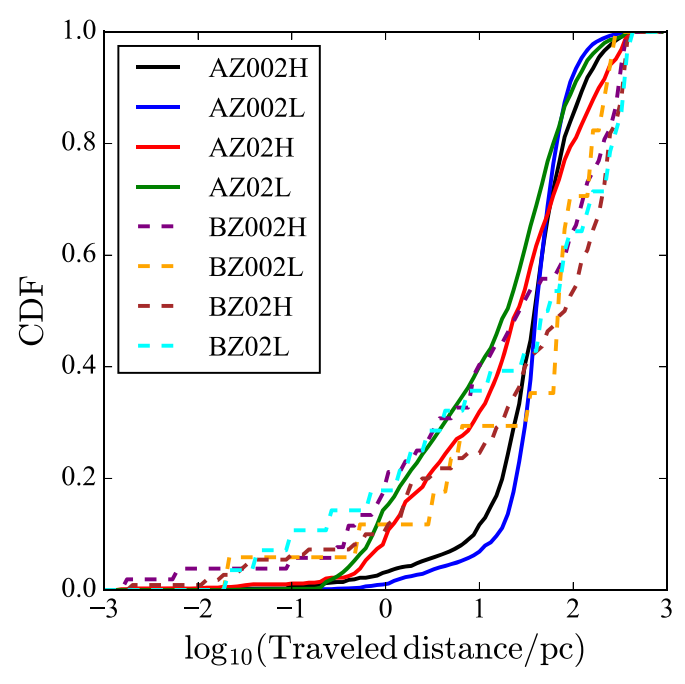


Figure 2. Cumulative distribution function of the distances traveled by the DNS candidates before they merge. Regardless of the model, most of the candidates merge before they travel more than 100 pc. This is well inside the potential well of the host halo and therefore a significant fraction of that the ejected *r*-process material is expected to be inherited by the subsequent star formation.

transfer—the so-called Case BB mass transfer phase—in which the NS accretes He from the He HG star (Delgado & Thomas 1981). Depending on the stars' masses at this stage and the binary's separation, this mass transfer may be either stable or unstable (Ivanova et al. 2003), and we consider the stable case in this section (For a detailed picture of this evolutionary channel, see Chruslinska et al. 2018, Figure 2).

From the population synthesis results, we find that systems going through this channel have separations $\approx R_{\odot}$ immediately prior to the second SN. DNSs formed through this channel comprise the bulk of the mostly green distributions in the bottom panels of Figure 1. In order to intuit the impact of natal kicks on the resulting DNSs, we show the distribution of merger times (after the second SN) in the top panel of Figure 3 for four different kick velocity distributions for a circular pre-SN orbit with an orbital separation of $1~R_{\odot}$. These are produced using the analytic formulation described in J. J. Andrews & A. Zezas (2019, in preparation) assuming NSs with masses of $1.4~M_{\odot}$ NSs and a $2.0~M_{\odot}$ pre-SN helium star mass.

Because of the strong dependence of the merger time on the DNS orbital separation ($t_{\rm merge} \sim a^4$), the merger time of DNSs formed through this scenario peaks at ≈ 100 Myr. Figure 3 indicates that merger times of <1 Myr are possible through this formation scenario, but only with relatively large kick velocities and then only at the tail of the distribution. These systems with short merger times are produced when "lucky" kicks pointed in the optimal direction (opposite of the orbital velocity), and produce DNSs with small orbital separations and large eccentricities. Since this channel requires large NS kick velocities, our low kick velocity models for submodel B produce fewer candidate DNSs than our high kick velocity models. However, regardless of the kick velocity applied, systems with merger times of ≈ 1 Myr are rare for systems formed through this evolutionary channel (for example, $\approx 1\%$

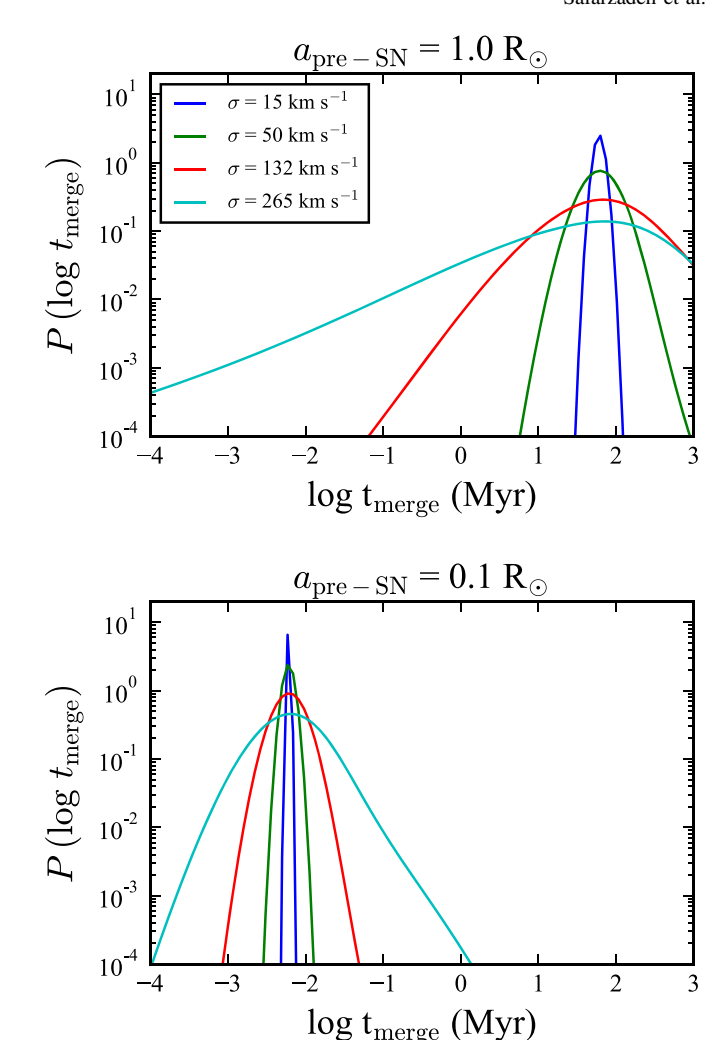


Figure 3. Merger time distribution (taken to be the time between DNS formation and merger) for systems with orbital separations characteristic of formation through an evolutionary channel with either stable (top panel) or unstable (bottom panel) Case BB mass transfer. The curves are computed analytically. For small kicks, the distributions are sharply peaked, while as the kick distributions increase, the merger time distributions broaden substantially. Formation of short merger time DNSs through the standard evolutionary channel (top panel) is only possible for systems formed with a large kick velocity, and then only for a small minority of systems at the tail of the distribution.

of all the DNSs in BZ002H). These fast-merging binaries form the types of DNS that can merge within a UFD and are denoted as purple points in submodel B. This channel exists in both submodels A and B. However, as we will show, submodel A provides yet another channel to produce our candidate DNSs.

4.2. The Unstable Case BB Mass Transfer Channel

Previous evolutionary simulations of mass transfer from a He HG star onto a NS (Dewi & Pols 2003; Ivanova et al. 2003) indicate that some systems, depending on the component masses and orbital period, should go through unstable Case BB mass transfer. However, the outcome of unstable Case BB mass transfer is uncertain; these systems enter into Roche lobe overflow as He HG stars, and as such, the donor stars in these systems lack clear core–envelope boundaries. For example, recent work by Vigna-Gómez et al. (2018) suggests that this Case BB phase ought to be predominantly stable to reproduce

the Galactic DNS population. Moreover, recent simulations suggest that this phase of mass transfer may be stable (Tauris et al. 2013, 2015; Lazarus et al. 2014). Nevertheless, uncertainty in the evolution of this phase has led us to test both submodel A, in which systems are allowed to survive unstable case BB mass transfer, and submodel B, in which such systems are forced to merge. Therefore the formation of DNSs through this evolutionary channel (for a detailed picture of this evolutionary channel, see Figure C1 in Chruslinska et al. 2018, and references therein), only occurs in our submodel A. The result of the binaries in submodel A that survive unstable case BB mass transfer is a tightly bound DNS with a separation of $\approx 0.1\,R_{\odot}$.

The bottom panel of Figure 3 shows the merger time distributions for DNSs with a pre-SN orbital separation of $0.1\,R_\odot$. For small kicks (relative to the orbital velocity), the NS natal kick only induces a relatively small perturbation on top of the orbit, leading to a sharply peaked merger time distribution at $\sim\!10^{-2}\,\mathrm{Myr}$. For larger kick velocity distributions, the merger time distribution broadens, as a larger range of DNS orbits become possible. Yet, despite the variation in the kick velocity distribution, the merger time is still strongly peaked between 10^{-3} and $10^{-1}\,\mathrm{Myr}$, and the corresponding fraction of candidate DNSs differs by less than a factor of two.

5. Comparing to Observations

In this section, we compare the total stellar mass needed to form in order to make one DNS candidate in the stellar mass content of the UFDs. The stellar mass content of Reticulum II is about $\approx 2.6^{+0.2}_{-0.2} \times 10^3 \, M_{\odot}$ (Bechtol et al. 2015), and the current estimate for Tucana III is about $\approx 8 \times 10^2 \, M_{\odot}$ (Drlica-Wagner et al. 2015), which makes it the lowest-luminosity UFD found to contain an r-I star (Hansen et al. 2017).

Despite their low masses today, there is evidence that these systems could have initially been more massive (Penarrubia et al. 2008). For instance, the observed tidal tails around Tucana III indicate that about 80% of the stellar mass is in the process of being tidally stripped (Li et al. 2018; Shipp et al. 2018), which would make the total stellar mass of Tucana III $\approx 4.6 \times 10^3 \, M_{\odot}$.

Figure 4 shows the stellar metallicity versus absolute visual magnitude of the MW's satellites (McConnachie 2012), where the V band absolute magnitudes of Tucana III and Reticulum II are -2.4 ± 0.42 (Drlica-Wagner et al. 2015) and -3.6 ± 0.1 (Bechtol et al. 2015). The corresponding metallicities of these two systems are -2.42 ± 0.07 (Simon et al. 2017), and -2.65 ± 0.07 (Simon et al. 2015). The flattening of the data toward lower luminosities has been attributed to tidal stripping (Fattahi et al. 2018).

The horizontal distance of the galaxies from this line could potentially indicate how much mass has been lost through tidal stripping in these systems, as tides do not affect the metallicities. The distances of the Tucana III and Reticulum II from the edge of the 3σ envelope could indicate the original stellar masses of these systems. Estimating the stellar mass loss due to tidal stripping by drawing a horizontal line in metallicity-stellar mass plane results in initial stellar masses of Reticulum II and Tucana III to be about a factor of 10 and 40 more massive in the past, respectively. Since these estimates are consistent with the location of these systems in the circular velocity, $V_{1/2}$, measured at the stellar half-mass-radius $(r_{1/2})$ versus $r_{1/2}$ plane (Fattahi et al. 2018), we use factors of 10 and

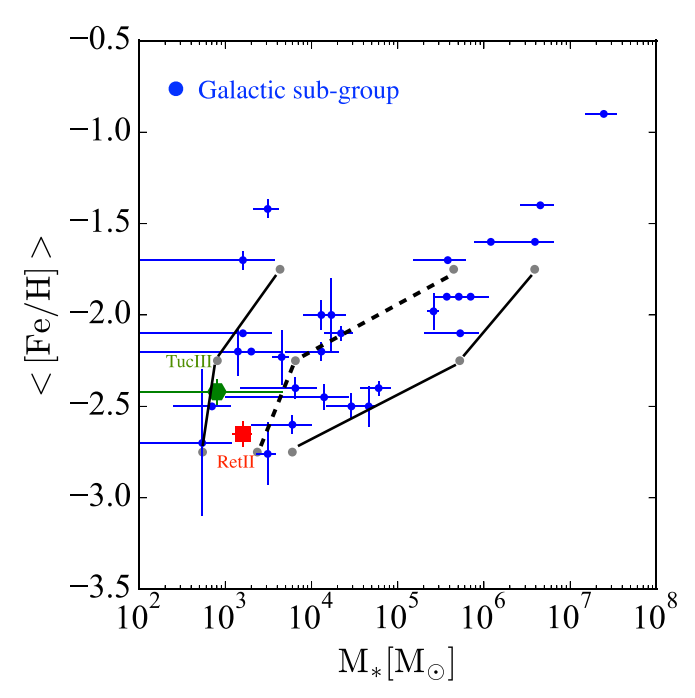


Figure 4. Shows the stellar metallicity vs. stellar mass of the MW's satellites in solid blue circles adopted from the McConnachie (2012) compilation, with updates from Fattahi et al. (2018). Tucana III and Reticulum II are shown with a red square and green hexagon, respectively, and their corresponding data are adopted from Drlica-Wagner et al. (2015) and Simon et al. (2017), and Bechtol et al. (2015) and Simon et al. (2015). The dashed line indicates the median value stellar mass for three different metallicity bins of -3 < [Fe/H] < -2.5, -2.5 < [Fe/H] < -2, and -2 < [Fe/H] < -1.5, while the solid lines encompass the 3σ envelope around the median. The horizontal distance of the galaxies from the right edge of the 3σ envelope could potentially indicate how much stellar mass in these systems has been lost through tidal stripping, assuming tides do not change the metallicities (Fattahi et al. 2018).

40 for the initial stellar masses of Reticulum II and Tucana III, respectively.

Figure 5 summarizes our results. Here, the black bars indicate the total stellar mass needed to form in order to make one candidate DNS in each model. The height of each bar indicates different assumptions about the virial radius of a UFD progenitor halo.

We have considered two cases of a $10^9 M_{\odot}$ halo with $r_{\rm vir} \approx 4.5$ kpc) at z=6, and a $10^8 M_{\odot}$ halo with $r_{\rm vir} \approx 1.3$ kpc at z=10. The required stellar mass in order to form a candidate DNS ranges from $10^5 M_{\odot}$ for submodel A to 10^7 for submodel B. Note that only a fraction (10%–20%) of UFDs within 100 kpc of the the MW's center are observed to be r-process-enriched.

To reflect this, the black bars in Figure 5 are lowered by 0.7 dex (assuming only about 20% of the UFDs are observed to be r-process-enriched) and are shown as red bars. In other words, although about $3 \times 10^5 \, M_\odot$ of stellar mass is needed to form in order to make one DNS candidate in the AZ002H model, a lower formation rate is possible since not all the UFDs are r-process-enriched.

The stellar masses of the two observed *r*-process UFDs are shown with shaded regions, where the width of the shaded regions for each of the satellites indicates the lower and upper limits on their stellar mass estimates after correcting for the stellar mass loss due to tidal stripping.

As illustrated in Figure 5, assuming these UFD systems have been tidally stripped, the predicted formation rate in submodel

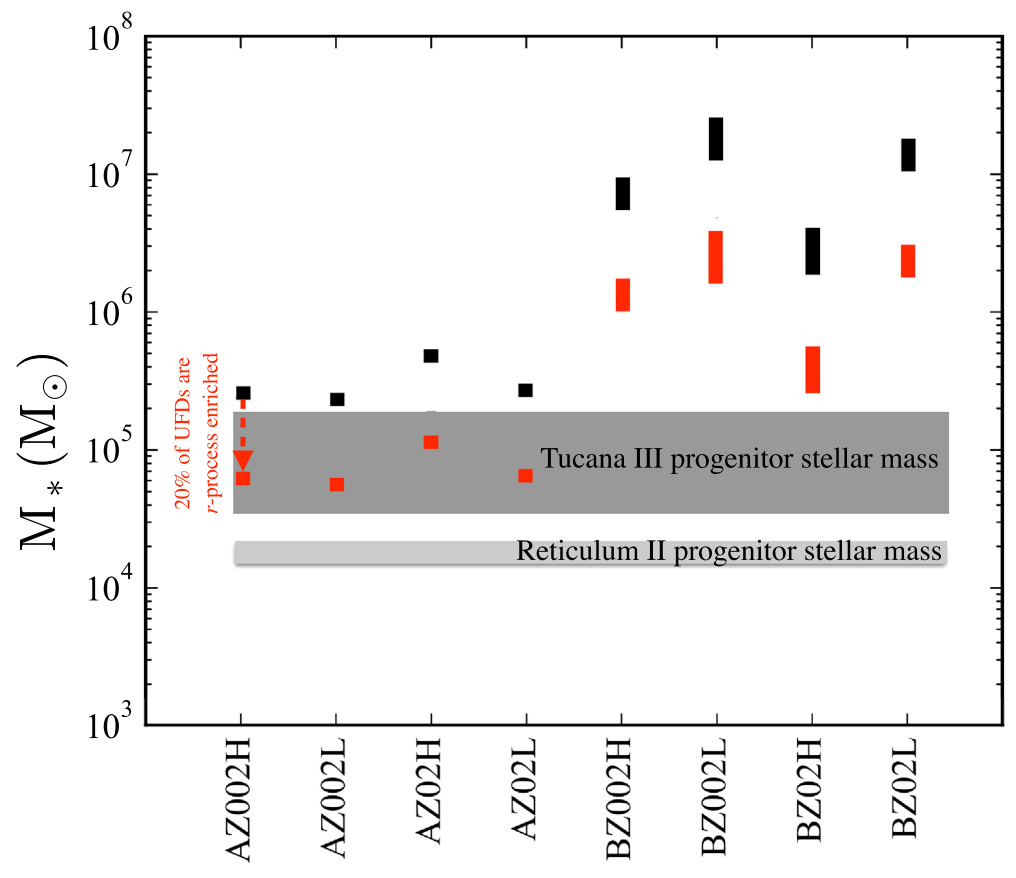


Figure 5. Formation rate of candidate NS binaries. Each black bar indicates the total mass of stars needed to form in order to have one candidate DNS. There are eight black lines corresponding to the right different models studied here. The models are described in Section 2.1. The length of each bar indicates the estimated birth rate of the candidates, depending on the halo mass in which we assume the DNS is born in. We have considered two cases of $10^9 M_{\odot}$ halo with $r_{\rm vir} \approx 4.5$ kpc) at z = 6, and $10^8 M_{\odot}$ with $r_{\rm vir} \approx 1.3$ kpc at z = 10 (Safarzadeh et al. 2018). The shaded regions indicate the estimated stellar mass of Reticulum II and Tucana III (Bechtol et al. 2015; Drlica-Wagner et al. 2015; Li et al. 2018; Shipp et al. 2018) after correcting for the tidal stripping mass loss. The downward thin red dashed arrow is 0.7 dex and indicates the fact that only about 20% of the total observed UFDs have been shown to be enriched in the r-process, therefore about an order of magnitude lower birth rates for the candidate DNSs are allowed. All the red bars are the black bars shifted downward by 0.7 dex.

A, where HG stars survive the CE phase, makes NSMs a plausible source of r-process enrichment in such systems. Although the estimated progenitor stellar mass of Reticulum II is a few factors below the red bars, this is still consistent with the overall picture we provide in this paper, because the estimated total stellar mass that needs to form in order to make 2×10^6 binaries based on the prescription in Dominik et al. (2012) can be lower than $2.8 \times 10^8 \, M_\odot$ by slight modifications to the model. Moreover, if Tucana III is a globular cluster and not a UFD, the red bars would need to be 1 dex lower than the black bars, which would make the results more consistent with Reticulum II.

6. Summary and Discussion

NSMs produce copious amount of *r*-process material, but it is difficult to reconcile the large natal kicks of NS binaries (DNSs) with the levels of *r*-process enrichment seen in UFD galaxies such as Reticulum II and Tucana III. Here, we have used a standard binary population synthesis model to identify a subset of DNSs whose *combination* of systemic center-of-mass velocities and merging times makes them merge well within the virial radius of their host halo, before they travel far from the star-forming region of their host galaxy.

The simulations have been carried out at different metallicity bins, different natal kick PDFs, and two different assumptions regarding unstable mass transfer with HG donors: submodel A considers the separation of the core and envelope in HG donor stars, while in submodel B this separation is not modeled, therefore a CE phase in submodel B always leads to merging of the compact object with the secondary stars' core. Due to this reason, a smaller percentage of all the compact binaries that are formed end up as NS binaries in submodel B relative to submodel A.

We conclude that only submodel A produces a population of DNSs that can r-process-enrich UFD-type galaxies, assuming, of course, that a large fraction of the r-process material ejected in an NSM event taking place well within the virial radius is recycled and will be locked in the stars formed after the event. In particular, one can form the candidate DNSs through a second phase of unstable mass transfer that shrinks the orbital separation to $\approx 0.1\,R_\odot$ and produces DNS merger timescales of <Myr after the second SN. Although DNSs formed in highly eccentric orbits are considered as candidates, their formation rate is very low and therefore would not make for a population that can explain r-process UFDs by themselves. Binaries that shrink to small orbital separations through a second phase of mass transfer are similar to the ultra-stripped helium stars (Tauris et al. 2017).

These results, however, rely on the assumption that more than 90% of the initial stellar mass of the observed *r*-process UFDs has been tidally stripped since entering the MW's halo

progenitor. The observations of Tucana III show that at least 80% of its stellar mass is being tidally stripped (Li et al. 2018; Shipp et al. 2018). Tidal stripping of satellites of a MW type halo has been studied extensively and it has been shown that a large fraction of stellar mass is indeed stripped away (e.g., see Penarrubia et al. 2008). However, the claim that these systems are tidally stripped could be challenging to prove theoretically. van den Bosch et al. (2018) showed that due to adiabatic resilience, the disruption of subhalos in the CDM paradigm is rare and even if the imparted energy to the subhalo exceeds its binding energy by a factor of 100, the subhalo still survives as a bound structure. Therefore, they claim that in the absence of baryonic processes all the disruptions of the subhalos in CDM simulations should be a numerical artifact. Although there are observations that support the tidal stripping scenario (Collins et al. 2017), future WFIRST observations of the field UFD galaxies that are free from tidal stripping scenarios can shed light on this matter.

On the other hand, recent deep *Hubble Space Telescope*/Advanced Camera for Surveys observations of the UFDs hint at the presence of a top-heavy IMF in such systems (Gennaro et al. 2018). This result is interesting in that de Mink & Belczynski (2015) have shown a more top-heavy IMF will lead to a factor of 2 or 3 increase in the overall formation of the NS binaries. Although this by itself is not enough to explain the observed statistics of the r-process-enhanced UFDs, it nevertheless helps to alleviate the tension. Moreover, as mentioned in the previous section, we have assumed that the total stellar mass budget of 2×10^6 binaries could be tweaked within a factor of 2 assuming different IMFs. This point could be rather crucial for the conclusions of this work because the red bars in Figure 5 stand above the stellar mass range of Ret-II.

Dynamical assembly in clusters at high redshifts has been proposed to produce tight DNSs (Ramirez-Ruiz et al. 2015) with short merging timescales. However, the small masses of UFDs disfavor a dynamical assembly origin for the candidate DNSs. Fast-merging channels in triple systems (Bonetti et al. 2018) could boost the merging rates, but the models analyzed in this work do not consider this channel. Separately, magnetorotationally driven (MRD) supernovae (Winteler et al. 2012; Nishimura et al. 2015; Wehmeyer et al. 2015; Mösta et al. 2018; Halevi & Mösta 2018) have been proposed to explain the observed high stellar abundances of Eu and Ba in such systems, because MRDs provide copious amount of r-process material. However, MRDs have been excluded from being a candidate because the evolution of [Mg/Fe] and [Ba/Fe] versus [Fe/H] in dwarf galaxies suggest different sources for α elements and r-process material (Duggan et al. 2018).

In this work, we have only considered models that are publicly available for analysis. These either have solar or 0.1 solar metallicities, while UFDs have metallicities of [Fe/H] < -2, which is 10 times lower than our lowest metallicity bin. The extrapolation of our results to lower metallicities might appear to be a stretch, as many aspects of stellar evolution are metallicity-dependent in a nonlinear way (e.g., stellar winds). However, DNS production efficiency either remains unchanged at lower metallicities or increases: Bramante & Linden (2016) showed that NS production efficiency is relatively unchanged when comparing the simulation with [Fe/H] = -2.3 to those with [Fe/H] = -1, and Chruslinska et al. (2018) showed that the merger rate of the DNSs increase in their standard model

when decreasing the metallicities from 0.1 solar to 0.01 solar (see their Table 2), which is in favor of our proposed model.

In the end, we need more complete models of fast-merging DNSs as r-process sources in UFDs. These would come from performing high-resolution zoom cosmological simulations on UFD host halos while modeling the candidate DNSs as r-process sources with their characteristic natal kicks and merging times. While we have shown in Safarzadeh & Scannapieco (2017) that a single NSM event can explain Reticulum II-like systems, these sets of simulations are vital to perform, otherwise the impact of natal kicks remains unclear. The ejected r-process material might not get effectively recycled into the new generation of stars (Macias & Ramirez-Ruiz 2018). This is because r-process material will be preferentially deposited in the halo and might get ejected before getting recycled. These simulations will predict the level of r-process enhancement, i.e., the ratio of different classes of r-process-enhanced stars to their parent category, which would be expected to observe in an ensemble of r-process UFDs if fast-merging NSMs are considered the source of r-process enrichment in the UFDs.

We are thankful to the referee for their careful reading of our work and helpful comments. We would like to thank Selma de Mink, Massimo Ricotti, Marla Geha, Frank van den Bosch, and David Radice for useful discussions. M.T.S. and J.J.A. are thankful to the Niels Bohr Institute for their hospitality, which made this work possible. J.J.A. acknowledges funding from the European Research Council under the European Union's Seventh Framework Program (FP/2007-2013)/ERC Grant Agreement n. 617001. M.T.S. and E.S. were supported by NASA theory grant NNX15AK82G. E.R. thanks the DNRF for support as a Niels Bohr Professor.

ORCID iDs

```
Mohammadtaher Safarzadeh https://orcid.org/0000-0002-1827-7011

Enrico Ramirez-Ruiz https://orcid.org/0000-0003-2558-3102

Jeff. J. Andrews https://orcid.org/0000-0001-5261-3923

Phillip Macias https://orcid.org/0000-0002-9946-4635
```

References

Evan Scannapieco https://orcid.org/0000-0002-3193-1196

```
Abbott, B. P., Abbott, R., Abbott, T. D., et al. 2017a, PhRvL, 119, 161101
Abbott, B. P., Abbott, R., Abbott, T. D., et al. 2017b, ApJL, 848, L12
Andrews, J. J., Farr, W. M., Kalogera, V., & Willems, B. 2015, ApJ, 801, 32
Bechtol, K., Drlica-Wagner, A., Balbinot, E., et al. 2015, ApJ, 807, 50
Beers, T. C., & Christlieb, N. 2005, ARA&A, 43, 531
Behroozi, P. S., Ramirez-Ruiz, E., & Fryer, C. L. 2014, ApJ, 792, 123
Belczynski, K., Bulik, T., Fryer, C. L., et al. 2010, ApJ, 714, 1217
Belczynski, K., Kalogera, V., & Bulik, T. 2002, ApJ, 572, 407
Belczynski, K., Kalogera, V., Rasio, F. A., et al. 2008, ApJS, 174, 223
Belczynski, K., Perna, R., Bulik, T., et al. 2006, ApJ, 648, 1110
Belczynski, K., Taam, R. E., Kalogera, V., Rasio, F. A., & Bulik, T. 2007, ApJ,
   662, 504
Beniamini, P., Hotokezaka, K., & Piran, T. 2016, ApJL, 829, L13
Bland-Hawthorn, J., Sutherland, R., & Webster, D. 2015, ApJ, 807, 154
Bonetti, M., Perego, A., Capelo, P. R., Dotti, M., & Miller, M. C. 2018, PASA,
   35, 124021
Bovill, M. S., & Ricotti, M. 2009, ApJ, 693, 1859
Bovill, M. S., & Ricotti, M. 2011, ApJ, 741, 17
Bramante, J., & Linden, T. 2016, ApJ, 826, 57
Brown, T. M., Tumlinson, J., Geha, M., et al. 2012, ApJL, 753, L21
```

Brown, T. M., Tumlinson, J., & Geha, M. 2014, ApJ, 796, 91

```
Chruslinska, M., Belczynski, K., Klencki, J., & Benacquista, M. 2018,
   MNRAS, 474, 2937
Collins, M. L. M., Tollerud, E. J., Sand, D. J., et al. 2017, MNRAS, 467, 573
Coulter, D. A., Foley, R. J., Kilpatrick, C. D., et al. 2017, Sci, 358, 1556
Delgado, A. J., & Thomas, H. C. 1981, A&A, 96, 142
Deloye, C. J., & Taam, R. E. 2010, ApJL, 719, L28
de Mink, S. E., & Belczynski, K. 2015, ApJ, 814, 58
Dewi, J. D. M., & Pols, O. R. 2003, MNRAS, 344, 629
Dominik, M., Belczynski, K., Fryer, C., et al. 2012, ApJ, 759, 52
Drlica-Wagner, A., Bechtol, K., Rykoff, E. S., et al. 2015, ApJ, 813, 109
Drout, M. R., Piro, A. L., Shappee, B. J., et al. 2017, Sci, 358, 1570
Duggan, G. E., Kirby, E. N., Andrievsky, S. M., & Korotin, S. A. 2018, ApJ,
Fattahi, A., Navarro, J. F., Frenk, C. S., et al. 2018, MNRAS, 476, 3816
Frebel, A., & Bromm, V. 2012, ApJ, 759, 115
Fryer, C. L., Belczynski, K., Wiktorowicz, G., et al. 2012, ApJ, 749, 91
Gennaro, M., Tchernyshyov, K., Brown, T. M., et al. 2018, ApJ, 855, 20
Giacobbo, N., & Mapelli, M. 2018, MNRAS, 480, 2011
Halevi, G., & Mösta, P. 2018, MNRAS, 477, 2366
Hansen, T. T., Simon, J. D., Marshall, J. L., et al. 2017, ApJ, 838, 44
Hobbs, G., Lorimer, D. R., Lyne, A. G., & Kramer, M. 2005, MNRAS,
Ivanova, N., Belczynski, K., Kalogera, V., Rasio, F. A., & Taam, R. E. 2003,
   ApJ, 592, 475
Janka, H.-T. 2017, ApJ, 837, 84
Ji, A. P., Frebel, A., Chiti, A., & Simon, J. D. 2016, Natur, 531, 610
Ji, A. P., Simon, J. D., Frebel, A., Venn, K. A., & Hansen, T. T. 2019, ApJ,
   870, 83
Kasen, D., Metzger, B., Barnes, J., Quataert, E., & Ramirez-Ruiz, E. 2017,
  Natur, 551, 80
Koposov, S. E., Belokurov, V., Torrealba, G., & Evans, N. W. 2015a, ApJ,
   805, 130
```

Koposov, S. E., Casey, A. R., Belokurov, V., et al. 2015b, ApJ, 811, 62

Kravtsov, A. V. 2013, ApJL, 764, L31

```
Lazarus, P., Tauris, T. M., Knispel, B., et al. 2014, MNRAS, 437, 1485
Li, T. S., Simon, J. D., Kuehn, K., et al. 2018, ApJ, 866, 22
Macias, P., & Ramirez-Ruiz, E. 2018, ApJ, 860, 89
MacLeod, M., & Ramirez-Ruiz, E. 2015, ApJL, 798, L19
Margutti, R., Alexander, K. D., Xie, X., et al. 2018, ApJL, 856, L18
McConnachie, A. W. 2012, AJ, 144, 4
Mösta, P., Roberts, L. F., Halevi, G., et al. 2018, ApJ, 864, 171
Nishimura, N., Takiwaki, T., & Thielemann, F.-K. 2015, ApJ, 810, 109
Penarrubia, J., Navarro, J. F., & McConnachie, A. W. 2008, ApJ, 673, 226
Pfahl, E., Rappaport, S., Podsiadlowski, P., & Spruit, H. 2002, ApJ, 574,
Ramirez-Ruiz, E., Trenti, M., MacLeod, M., et al. 2015, ApJL, 802, L22
Safarzadeh, M., & Côté, B. 2017, MNRAS, 471, 4488
Safarzadeh, M., Ji, A. P., Dooley, G. A., et al. 2018, MNRAS, 476, 5006
Safarzadeh, M., & Scannapieco, E. 2017, MNRAS, 471, 2088
Shipp, N., Drlica-Wagner, A., Balbinot, E., et al. 2018, ApJ, 862, 114
Simon, J. D., Drlica-Wagner, A., Li, T. S., et al. 2015, ApJ, 808, 95
Simon, J. D., & Geha, M. 2007, ApJ, 670, 313
Simon, J. D., Li, T. S., Drlica-Wagner, A., et al. 2017, ApJ, 838, 11
Tauris, T. M., Kramer, M., Freire, P. C. C., et al. 2017, ApJ, 846, 170
Tauris, T. M., Langer, N., Moriya, T. J., et al. 2013, ApJL, 778, L23
Tauris, T. M., Langer, N., & Podsiadlowski, P. 2015, MNRAS, 451, 2123
van den Bosch, F. C., Ogiya, G., Hahn, O., & Burkert, A. 2018, MNRAS,
  474, 3043
van den Heuvel, E. P. J. 2007, in AIP Conf. Ser. 924. The Multicolored
   Landscape of Compact Objects and Their Explosive Origins, ed. T. di Salvo
   (Melville, NY: AIP), 598
Vargas, L. C., Geha, M., Kirby, E. N., & Simon, J. D. 2013, ApJ, 767, 134
Verbunt, F., Igoshev, A., & Cator, E. 2017, A&A, 608, A57
Vigna-Gómez, A., Neijssel, C. J., Stevenson, S., et al. 2018, MNRAS,
   481, 4009
Wehmeyer, B., Pignatari, M., & Thielemann, F. K. 2015, MNRAS, 452, 1970
Weisz, D. R., Dolphin, A. E., Skillman, E. D., et al. 2014, ApJ, 789, 148
Winteler, C., Käppeli, R., Perego, A., et al. 2012, ApJL, 750, L22
```